AGU PUBLICATIONS

Geochemistry, Geophysics, Geosystems

RESEARCH ARTICLE
10.1002/2016GC006627

Special Section:
Magnetism From Atomic to Planetary Scales: Physical Principles and Interdisciplinary Applications in Geo- and Planetary Sciences

Holocene glacial activity in Barilari Bay, west Antarctic Peninsula, tracked by magnetic mineral assemblages: Linking ice, ocean, and atmosphere

Brendan T. Reilly[1,2], Carl J. Natter Jr.[1,3], and Stefanie A. Brachfeld[1]

[1]Department of Earth and Environmental Studies, Montclair State University, Upper Montclair, New Jersey, USA, [2]College of Earth, Ocean, and Atmospheric Sciences, Oregon State University, Corvallis, Oregon, USA, [3]Kleinfelder Inc., Hamilton, New Jersey, USA

Key Points:
- Western Antarctic Peninsula detrital magnetic mineral assemblages are studied as tracers of lithogenic sediments
- Distinct magnetic signatures of sedimentary facies exist for sea ice, subice shelf, and grounding-line environments
- Magnetic mineral provenance, within sedimentologic context, provide insight to late Holocene glacial activity

Supporting Information:
- Figure S1
- Tables S1–S13

Correspondence to:
B. T. Reilly,
breilly@coas.oregonstate.edu

Citation:
Reilly, B. T., C. J. Natter, and S. A. Brachfeld (2016), Holocene glacial activity in Barilari Bay, west Antarctic Peninsula, tracked by magnetic mineral assemblages: Linking ice, ocean, and atmosphere, *Geochem. Geophys. Geosyst.*, *17*, 4553–4565, doi:10.1002/2016GC006627.

Received 6 SEP 2016
Accepted 25 OCT 2016
Accepted article online 1 NOV 2016
Published online 16 NOV 2016

Abstract We investigate the origin and fate of lithogenic sediments using magnetic mineral assemblages in Barilari Bay, west Antarctic Peninsula (AP) from sediment cores recovered during the Larsen Ice Shelf System, Antarctica (LARISSA) NBP10-01 cruise. To quantify and reconstruct Holocene changes in covarying magnetic mineral assemblages, we adopt an unsupervised mathematical unmixing strategy and apply it to measurements of magnetic susceptibility as a function of increasing temperature. Comparisons of the unmixed end-members with magnetic observations of northwestern AP bedrock and the spatial distribution of magnetic mineral assemblages within the fjord, allow us to identify source regions, including signatures for "inner bay," "outer bay," and "northwestern AP" sources. We find strong evidence that supports the establishment of a late Holocene ice shelf in the fjord coeval with the Little Ice Age. Additionally, we present new evidence for late Holocene sensitivity to conditions akin to positive mean Southern Annual Mode states for western AP glaciers at their advanced Neoglacial positions.

1. Introduction

Abrupt climate change on the Antarctic Peninsula (AP) in the past several decades, manifested through increasing atmospheric temperature and catastrophic ice shelf disintegration, has validated the importance of studying mechanisms and impacts of AP environmental change [*Smith et al*., 1999; *Domack et al*., 2001; *Scambos et al*., 2003; *Vaughan*, 2006; *Hulbe et al*., 2008; *Bentley et al*., 2009]. To investigate these recent changes and their paleoenvironmental context, the interdisciplinary LARsen Ice Shelf System Antarctica (LARISSA) 2010 field season visited the western AP [see N. B. Palmer 2010–01 Cruise Report, 4 January–2 March, *Domack and the LARISSA Science Party*, 2010], a region which on Holocene timescales is especially sensitive to variations in the position and intensity of zonal westerly winds and coastal upwelling intensity of warm upper circumpolar deep water (UCDW) [*Bentley et al*., 2009, and references therein]. A suite of sediment cores recovered from Barilari Bay record a detailed late Holocene paleoenvironmental history, including the expression and timing of a late Holocene glacial advance roughly coeval with the Little Ice Age (LIA) as expressed in the Northern Hemisphere [*Christ et al*., 2014].

In this study, we investigate the terrigenous component of the fjord sediments using their magnetic properties and compare these to observations of northwestern AP bedrock samples. Sediment bulk magnetic properties, a function of magnetic mineralogy, magnetic grain-size, and the concentration of magnetic minerals, reflect a combination of depositional processes, sediment provenance, and diagenesis [*Verosub and Roberts*, 1995; *Liu et al*., 2012]. Magnetic minerals, as tracers of terrigenous sediments, have been demonstrated to be particularly useful in the study of past glacial activity [*Stoner et al*., 1995, 1996; *Sagnotti et al*., 1998; *Brachfeld and Banerjee*, 2000; *Brachfeld et al*., 2002, 2013; *Jovane and Verosub*, 2011; *Venuti et al*., 2011; *Roberts et al*., 2013], as fingerprints of terrestrial source material [*Brachfeld et al*., 2002, 2004, 2013; *Cowan et al*., 2006; *Hatfield et al*., 2013], and for understanding of the Holocene paleoenvironmental history of the AP [*Leventer et al*., 1996; *Brachfeld et al*., 2002].

To separate bulk magnetic properties of sediment samples and better understand what drives environmental magnetic signals, researchers have employed strategies that include mathematical end-member modeling of a variety of magnetic measurements [*Heslop and Dillon*, 2007; *Heslop and Roberts*, 2012; *Heslop*, 2015;

Lascu et al., 2015] and particle size specific magnetic measurements [*Hatfield et al.*, 2013; *Hatfield*, 2014; *Razik et al.*, 2014]. Here we adopt an unsupervised unmixing minimum volume simplex analysis to decompose covarying magnetic mineral assemblages, as tracked by the temperature dependence of magnetic susceptibility, and determine each end-member's contribution to magnetic susceptibility. This decomposed signal is then interpreted through comparison to local bedrock samples and the spatial distribution of magnetic mineral assemblages in the fjord.

2. Study Area

Barilari Bay, a western AP fjord visited during the LARISSA NBP10-01 cruise, is located upwind of and at the same latitude as the former Larsen B ice shelf, allowing for east-west comparison of Holocene glacial response to oceanic and atmospheric forcing (Figure 1). Historical and geologic studies both indicate that while eastern AP changes are driven by atmospheric forcing, as demonstrated by the Holocene history and unprecedented breakup of the Larsen B ice shelf [*Scambos et al.*, 2003; *Domack et al.*, 2005; *Rebesco et al.*, 2014], the western AP is particularly sensitive to oceanographic forcing [*Cook et al.*, 2016], with high resolution records suggesting variable and episodic incursion of UCDW in the late Holocene [*Ishman and Sperling*, 2002; *Shevenell and Kennett*, 2002; *Bentley et al.*, 2009; *Peck et al.*, 2015].

The bathymetry of the fjord, charted by multibeam survey during NBP10-01, identifies a series of glacially carved basins and historic grounding lines (Figure 2) [*Christ et al.*, 2014]. The NBP10-01 sediment core suite

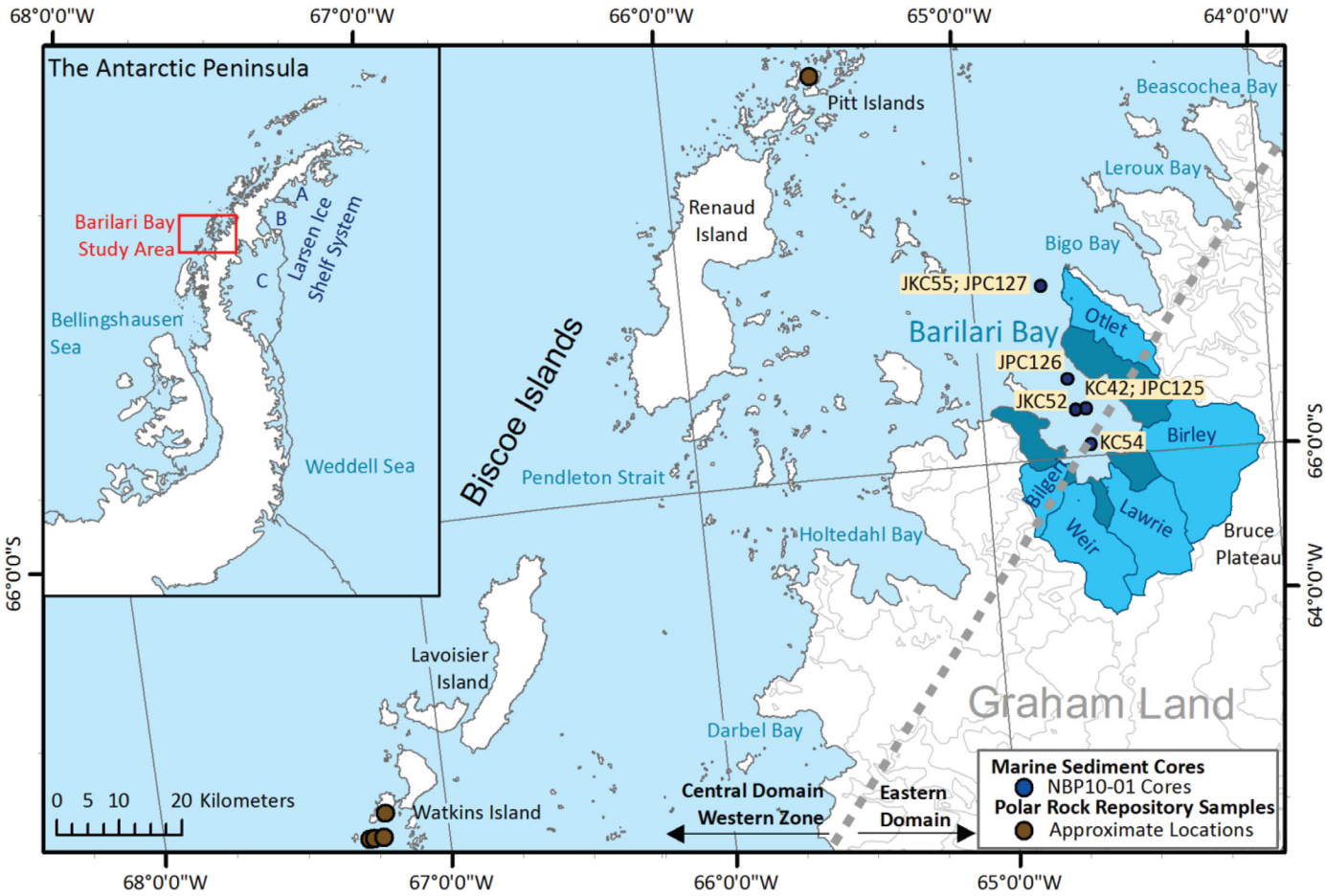

Figure 1. Map of the Barilari Bay region, western Antarctic Peninsula, including the locations of cores recovered during NBP10-01 (blue circles) and new Polar Rock Repository samples analyzed for this study (brown circles). Contour lines indicate 500 m elevation. The blue area surrounding Barilari Bay indicates the drainage areas for glaciers terminating in the bay, with the five major glaciers—Otlet, Birely, Lawrie, Weir, and Bilgeri—indicated in lighter blue. Elevation contours and glacial drainage delineations were determined from an Antarctic Peninsula digital elevation model [*Cook et al.*, 2012]. The gray dashed line indicates the approximate terrane boundary between the Central Domain Western Zone and the Eastern Domain [*Ferraccioli et al.*, 2006].

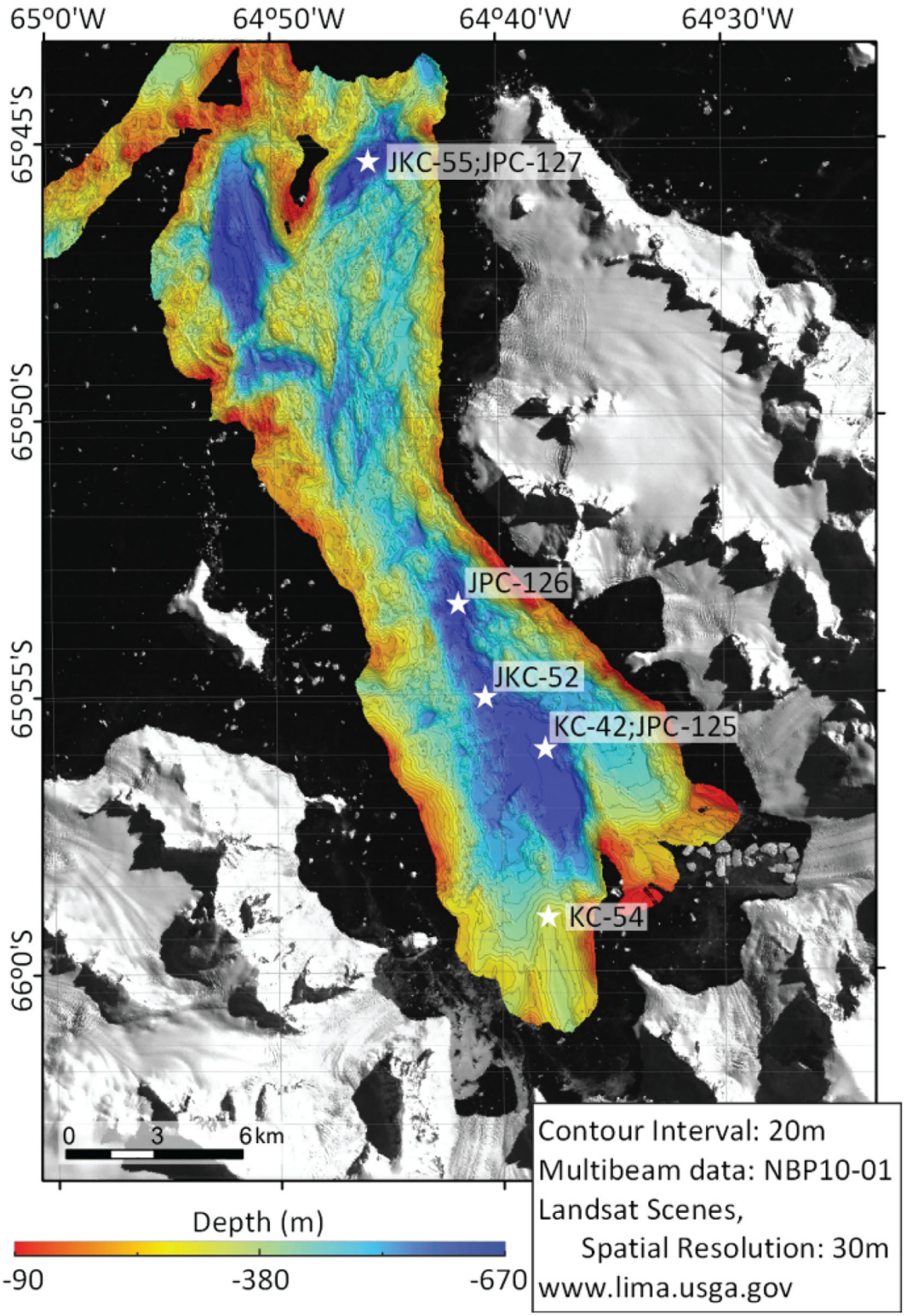

Figure 2. Bathymetry of Barilari Bay with NBP10-01 core locations [after *Christ et al*., 2014].

sampled three unique sedimentary basins, including the inner-most (KC-42, JPC-125, JKC-52), middle (JPC-126), and outer-most basins (JKC-55, JPC-127) (Table 1) [*Christ et al*., 2014]. Additionally, KC-54, the most ice-proximal core, was recovered from the historic grounding-line wedge [*Christ et al*., 2014]. Five named

Table 1. NBP10-01 Marine Sediment Cores

Core	Length (cm)	Latitude	Longitude	Water Depth (m)
KC-42	130	65°56.44′S	64°38.26′W	610
KC-54	133	65°59.05′S	64°37.90′W	341
JKC-52	599	65°36.05′S	64°40.60′W	595
JKC-55	426	65°45.38′S	64°45.64′W	652
JPC-125	2125	65°55.99′S	64°38.40′W	610
JPC-126	2146	65°53.41′S	64°41.79′W	642
JPC-127	868	65°45.36′S	64°45.64′W	653

glaciers terminate in the bay—Otlet, Birley, Lawrie, Weir, and Bilgeri glaciers—along with a number of smaller, unnamed glaciers (Figure 1). Historically, Barilari Bay was the southernmost drainage for the Hugo Island Trough [*Lavoie et al*., 2015], sharing a deep bathymetric conduit across the shelf for UCDW with the Palmer Deep (Ocean Drilling Program Site 1098) [*Domack et al*., 2001].

Chronologies for cores KC-54, JPC-126, and JKC-55 are given in *Christ et al*. [2014] and are based on a combination of ^{137}Cs, ^{210}Pb, and ^{14}C dating. A magnetic susceptibility low near the base of JKC-55 is dated at 3863 cal. yr BP (250–252 cm) and is consistent in timing with the Middle Holocene Hypsithermal as observed elsewhere on the AP [*Domack et al*., 2001; *Bentley et al*., 2009]. Neoglacial cooling follows around 2815 cal. yr BP and primary productivity declines while sea ice coverage increases. Low %TOC and finer particle sizes beginning around 626 cal. yr BP (80–84 cm) and ending around 82 cal. yr BP (19–24 cm) are interpreted as reflecting the establishment of an LIA ice shelf in Barilari Bay coincident in timing with anomalously cold Holocene atmospheric temperatures at the WAIS divide ice core site [*Orsi et al*., 2012; *WAIS Divide Project Members*, 2013; *Christ et al*., 2014]. This is supported by middle and inner bay lithologic changes consistent with facies models for ice shelf and glaciomarine sedimentation, including a change from seasonally open marine to high accumulation, grounding-line proximal sediments, indicating glacial advance about 730 cal. yr BP in JPC-126 and a transition from a diamict to subice shelf facies indicating a grounding-line "back-off" event occurring before 252 cal. yr BP in KC-54 [*Domack and Ishman*, 1993; *Domack and Harris*, 1998; *Christ et al*., 2014].

The bedrock geology in and around Barilari Bay has not been extensively studied, with only limited field study of the offshore Biscoe Islands [*Smellie et al*., 1985; *Moyes*, 1986]. Described outcrops of igneous rocks can broadly be interpreted as associated with the Cretaceous-Tertiary Andean Intrusive Suite or Jurassic Volcanic Rocks (supporting information Figure S1a). The general subice geology can be inferred from the regional tectonic history [*Elliot*, 1975; *Burton-Johnson and Riley*, 2015] and implications for detrital magnetic mineralogy can be inferred from comparison of bedrock magnetic susceptibilities with aeromagnetic geophysical surveys [*Wendt et al*., 2013]. Magnetic anomalies from geophysical surveys indicate Barilari Bay sits on the boundary of two geologic terranes: the Mesozoic magmatic arc dominated Central Domain to the west and the Trinity Peninsula Group dominated Eastern Domain, composed of the mostly sedimentary and metasedimentary rocks of the deformed Gondwana continental margin, to the east [*Ferraccioli et al*., 2006; *Golynsky et al*., 2013].

Bedrock samples from the Eastern Domain have the lowest mean magnetic susceptibility of any rock group on the AP, and arc-related igneous rocks contain low concentrations of magnetite, likely due to magmatic redox conditions [*Wendt et al*., 2013]. Bedrock samples from the Central Domain include arc-related intrusive rocks from the Cretaceous-Tertiary Andean intrusive suite that have the highest mean magnetic susceptibility values for measured rock samples on the AP [*Wendt et al*., 2013]. These sources are likely the most important source for detrital magnetic mineral assemblages in Barilari Bay and the northwestern AP, despite common sedimentary and metasedimentary lithic fragments and drop stones found in Western AP shelf sediments [*Brachfeld et al*., 2004; *Reilly*, 2013; *Wendt et al*., 2013].

3. Materials and Methods

3.1. U.S. Polar Rock Repository Samples

Bedrock samples from the Biscoe Islands were loaned from the U.S. Polar Rock Repository (PRR) at the Byrd Polar Research Center, Ohio State University. Samples were chosen based on proximity of available samples to Barilari Bay (none were available within the bay itself), and an attempt to represent regional lithologies including gabbros, tonalities, volcaniclastics, and chert (Figure 1; supporting information Table S1). Rock chips from the PRR samples were mounted in epoxy and polished and observed using a Hitachi S-3400N scanning electron microscope (SEM) and Bruker X-flash energy dispersive spectrometer (EDS).

3.2. Marine Sediment Cores

Discrete subsamples (with sampling horizon 1 cm thick) from kasten cores were collected onboard ship at 1, 2, or 5 cm intervals. Discrete samples were collected at 5 cm intervals from jumbo piston cores, which were opened at the Antarctic Marine Geology Research Facility at Florida State University. The disturbed upper 178 cm in JPC-126 was only sampled every 20 cm. Samples were freeze-dried and packed into gelatin capsules for magnetic analyses. A composite depth scale for the outer Barilari Bay cores, JKC-55 and JPC-127, was determined by correlating their magnetic susceptibility profiles. JKC-55 recovered the sediment water interface and was used as the reference core. A constant 5 cm offset was used for JTC-127 relative to JKC-55. The Analyseries 2.0.4 software [*Paillard et al*., 1996] was used to adjust the depth scale of JPC-127 relative to JKC-55 (composite depth scale in supporting information Tables S12 and S13).

At select intervals where sufficient coarse material was available (i.e., bases of turbidites, diamict, inner-bay seasonally open marine facies), clasts >0.5 mm were prepared as thin sections by Mineral Optics Laboratory for optical microscopy and lithology identification via point counting on a Zeiss Aksioskop.

3.3. Magnetic Analyses

Mass normalized low-field magnetic susceptibility (χ_{lf}) and thermomagnetic curves (χ(T)) were measured on an AGICO KLY-4 Kappabridge. Thermomagnetic curves were measured between room temperature and 700°C in a flowing argon atmosphere during heating and cooling. Hysteresis parameters were measured on a Princeton Measurements Corporation MicroMag 3900 Vibrating Sample Magnetometer (VSM) in a 1 T peak field (H). Rock chips (~50–150 mg) were immobilized with quartz Fiberfrax® inside gelatin capsules. Hysteresis loops were mass normalized and the high-field slope of the M-H curve (χ_{hf}) was calculated using the induced magnetization values between 0.7 and 1 T. χ_{hf} was then used to remove the diamagnetic and paramagnetic contributions to the induced magnetization. Saturation magnetization (M_s), saturation remanence (M_r), and bulk coercivity (H_c) were determined from the diamagnetic/paramagnetic corrected hysteresis loops. The coercivity of remanence (H_{cr}) was determined from the DC demagnetization of an initial 1 T IRM. The S-ratio was determined by applying an initial field of 1 T, followed by a back-field of −300 mT (IRM_{-300T}) and normalizing the IRM_{-300mT} by the 1 T IRM [*Stober and Thompson*, 1979].

3.4. End-Member Modeling of Temperature-Dependent Susceptibility

End-member modeling of χ(T) takes the form:

$$X = AS + E, \text{ subject to } A \geq 0 \text{ and } A1_p = 1,$$

where X is a matrix of χ values containing n rows (1 per sample) and l columns (1 per temperature step), A is a matrix of the fractional abundance of the end-members of n rows and p columns (1 per end-member), S is a matrix the end-member composition in p rows and l column, E is an error matrix to be minimized, and 1_p is a column vector of ones of length p [*Heslop*, 2015]. The nonnegativity and sum-to-one constraints on A ensure the modeled end-member abundances are physically meaningful. The temperature derivative of 82 χ(T) curves (dχ/dT) from KC-54 (n = 4), JPC-125 (n = 2), JPC-126 (n = 20), TC-126 (n = 10), and JPC127 (n = 44) were placed in matrix X after resampling χ(T) at 3°C steps between 50 and 698°C. We use the temperature derivative, as the magnetic minerals are most effectively identified by temperatures of the greatest change in χ. Although χ(T) was measured in an argon atmosphere, irreversibility upon cooling suggests some alteration occurred above the Curie point of magnetite (~580°C), perhaps due to variable organic carbon concentration or alteration of clay minerals. Accordingly, this analysis was only performed on the heating curves, which we interpret as representative of the detrital assemblage. Heating curves were normalized by χ at 50°C to account for changes in magnetic mineral concentration so that our end-member model tracks changes in relative contribution.

This end-member modeling approach assumes linear additivity of χ at each temperature step (i.e., for any given T, $\chi_{EM1} + \chi_{EM2} + \chi_{EM3} = \chi_{Bulk}$). This is likely a valid assumption as magnetic interactions are expected to be negligible on χ_{lf} and χ_{lf} has been demonstrated as reliably linearly additive in laboratory tests [*Lees*, 1997]. It is important to note, end-member modeling will not necessarily isolate pure magnetic mineral phases (e.g., magnetite, hematite); rather, this end-member modeling will isolate covarying magnetic mineral assemblages that can be interpreted within the context of geologically meaningful end-members.

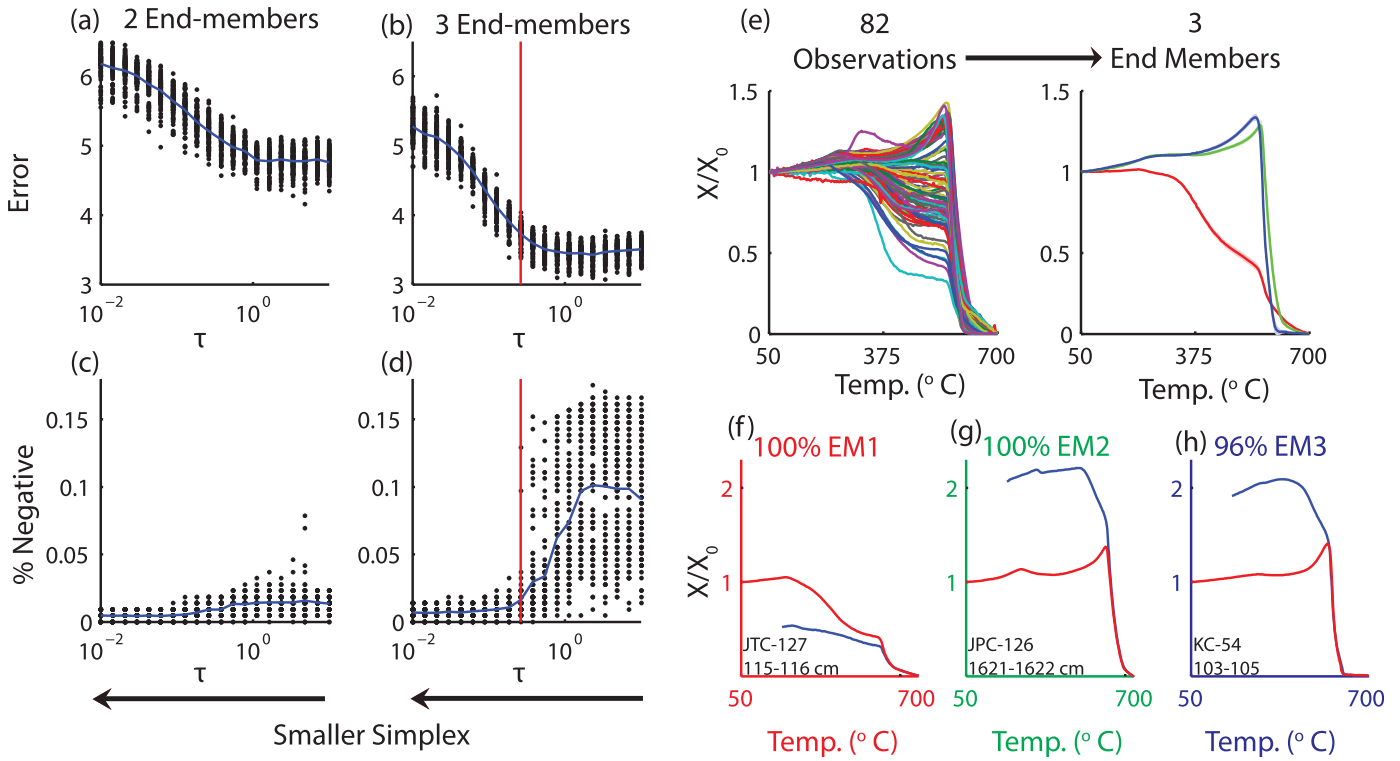

Figure 3. End-member model selection for 100 iterations of two and three end-member scenarios, including (a and b) error and (c and d) shape constraint for a range of regularization parameters (τ; see text for discussion). The selected model reported here is indicated by the vertical red line. (e) The model uses the temperature derivative of 82 χ(T) curves from four sediment cores and defines three covarying magnetic mineral assemblages, which can be interpreted through comparison with measured χ(T) curves. (f–h) Representative χ(T) curves that are dominated by each end-member, representing maghemite dominated assemblages (EM1) and magnetite dominated assemblages with variable cation substitution (EM2 and EM3). End-member curves are available in supporting information Table S2.

To define the end-members that compose matrix S so that we can solve for A by minimizing the sum of squares in E, we employ an unsupervised unmixing minimum volume simplex analysis using the Simplex Identification via Split Augmented Lagrangian (SISAL) routine [*Bioucas-Dias*, 2009] and adopting the method by *Heslop and Roberts* [2012] to χ(T). The SISAL routine is robust to outliers by using a soft constraint on negativity in matrix A, controlled by the regularization parameter, τ. The resulting end-members represent the vertices of the $p-1$ dimensional simplex that bounds the data, where p is equal to the number of end-members. Progressively smaller values of τ result in a smaller bounding simplex, by allowing progressively more data to lie outside the simplex (see Figure 18 in *Heslop* [2015] for conceptual illustration).

To determine the appropriate value of τ (i.e., the size of the bounding simplex) and define matrix S, we run 100 iterations of 70 randomly selected $d\chi/dT$ curves at 20 log distributed τ values (10^{-2}–10^{1}) and 2 and 3 end-member scenarios. To monitor for realistic χ(T) curve shapes, we calculate the percentage of negative χ values in the integrated $d\chi/dT$ end-member curves ($\chi(50°C) = 1$). Error is calculated as the square root of the sum of squares in error matrix E. The final end-members are defined as the mean of the 100 iterations (Figures 3a–3d).

4. Results

4.1. Magnetic Mineral Assemblages

We identify three major covarying magnetic mineral end-member assemblages (EM1–3) present in Barilari Bay (Figure 3e; supporting information Tables S2 and S3). We choose a three end-member model with the smallest simplex that preserves realistic χ(T) and with an acceptable error-level ($\tau = 0.26$), because it explains significant additional variance when compared to the two end-member scenario and all three end-members can be explained in a geologically meaningful way when compared to bedrock geology and fjord sediment distribution (see sections 4.2 and 4.3). Additional end-members scenarios only provide minor

reductions in the model error. Magnetic mineralogy is determined by the identification of Curie temperatures, which represent the order-disorder (ferromagnetic-paramagnetic) transition, and characteristic alteration with temperature.

EM1 is a mixture of maghemite and magnetite. Maghemite is identified by its inversion to hematite at high temperatures, manifested by cooling curves that are weaker than heating curves in all samples that contain EM1 in significant proportions [*Özdemir and Banerjee*, 1984; *Gehring et al.*, 2009]. EM2 and EM3 are similar and reflect magnetite as the dominant magnetic mineral; however, they are differentiated by differences in Curie temperature, with EM2 Curie temperature at about 584°C and EM3 Curie temperature around 572°C. This difference in Curie temperature can be attributed to cation replacement or oxidation [*Lattard et al.*, 2006]. This difference in Curie temperatures, although subtle, is justified by bedrock Curie temperature observations (see section 4.2). Cooling curves in samples dominated by EM2 and EM3 are greater than their heating curve, indicating some alteration of another mineral at high temperatures (Figures 3g and 3h). Hematite, identified by a continued drop in χ above the Curie point for magnetite, is present in EM1 and EM2. However, it is possible that its presence in EM1 is a product of maghemite inversion.

4.2. Bedrock Geology

Lithic grain counts made on fjord sediments, where sufficient coarse fraction (>0.5 mm) was available, show sedimentary and metasedimentary grains, likely of the Trinity Peninsula Suite, comprise at least 2/3 of the lithic assemblage and indicate that, while the plutonic rocks are likely the most important contributors to the detrital magnetic mineral assemblages [e.g., *Brachfeld et al.*, 2004; *Wendt et al.*, 2013] they are volumetrically less significant for the total lithogenic assemblage (supporting information Figure S1b).

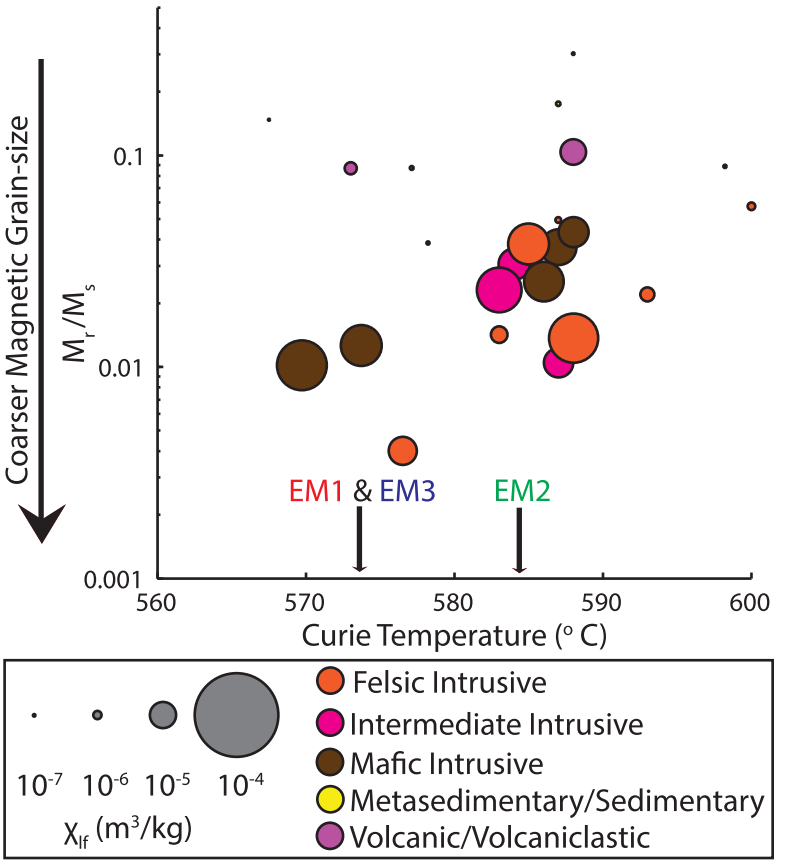

Figure 4. Summary of bedrock magnetic observations from this study and *Brachfeld et al.* [2004], with the size of the point proportional to the bedrock χ_{lf} and color-coded to their simplified lithology. End-member Curie temperatures from Barilari Bay sediments are also indicated. Detailed magnetic data are available in supporting information Table S1.

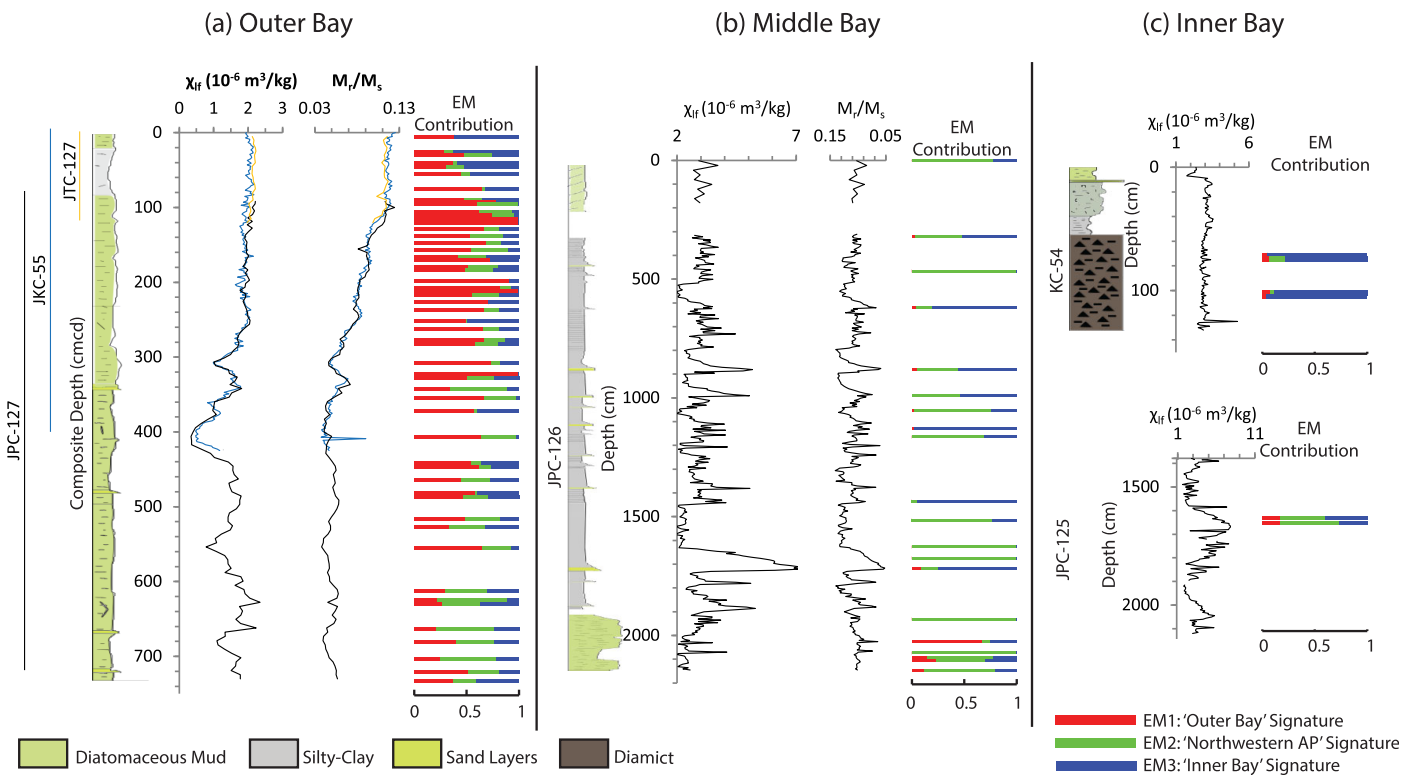

Figure 5. Summary of magnetic mineral assemblages for (a) outer bay cores, (b) middle bay cores, and (c) inner bay cores, including χ_{lf}, a proxy for magnetic mineral concentration, M_r/M_s, a proxy for magnetic mineral grain-size, and relative end-member abundance of EM1 (red), EM2 (green), and EM3 (blue) magnetic mineral assemblages. Lithologic logs are generalized from *Christ et al*. [2014]. Detailed magnetic data are available in supporting information Tables S3–S13.

Magnetic analysis of PRR samples from the Biscoe Islands are consistent with previous results reported from the Northwestern AP [*Brachfeld et al*., 2004]. Rocks with high magnetic susceptibility, and thus important for detrital magnetic mineral assemblages, found on the AP can be grouped into two categories, finer (but still coarse multidomain) magnetite with high Curie temperatures (580–590°C) and coarser magnetite with lower Curie temperatures (565–575°C) (Figure 4). These Curie temperature ranges agree well with those determined for EM2 and EM3. We also note that even though these bedrock observations are limited, it appears that the higher Curie temperature group is much more common for bedrock in the northwestern AP. SEM observation of PRR samples are consistent with magnetic observations, with pluton rocks of the Cretaceous-Andean Intrusive Suite containing common and large Fe-Ti oxides (supporting information Figures S1c–S1g).

4.3. Marine Sediment Cores

Bulk magnetic properties and χ(T) unmixing results for inner, middle, and outer Barilari Bay cores are provided in supporting information Tables S3–S13 and summarized in Figure 5. These results are discussed here with respect to three glaciomarine facies found in the bay: grounding line, sea ice/seasonally open marine, and edge-proximal ice shelf. An additional diamict facies is found at the base of KC-54, which contains almost exclusively an EM3 assemblage of magnetic minerals. A detailed discussion of the sedimentology of these facies for cores KC-54, JPC-126, and JKC-55 can be found in *Christ et al*. [2014].

4.3.1. Grounding-Line Facies

Grounding-line facies in Barilari Bay consist of organic poor, well graded silts/sands and/or rhythmically laminated sections from grounding-line plume, undermelt, and turbidite deposits. These deposits are found in JKC-52, JKC-42, JPC-125, and JPC-126 from the inner and middle sedimentary basins.

Magnetic mineral concentration (tracked by χ_{lf}) and magnetic mineral grain-size (tracked by concentration independent parameters M_r/M_s and H_{cr}/H_c) are highly variable, with high concentrations of coarse magnetic minerals at the coarse silt/sand at the base of turbidites and lower concentrations of finer magnetic

minerals in the homogenous silty muds at the top of turbidites, indicating hydrodynamic sorting of magnetic minerals by density and grain-size.

Magnetic mineralogy varies between EM2 and EM3; however, their occurrence in the same turbidites suggest their distribution is also driven by sediment transport and sorting and not solely provenance. High proportions of EM3 are found at the sandy bases of turbidites, consistent with the coarser magnetic minerals found at similar Curie points in Northwestern AP bedrock samples. A high-coercivity mineral, tracked by the S-ratio, is also concentrated at the base of these turbidites and also likely influences the χ_{hf}, calculated between 0.7 and 1 T, for if a mineral like hematite was present in significant quantity it would not saturate in the 1 T field [*Brachfeld*, 2006].

4.3.2. Sea Ice/Seasonally Open Marine Facies

Seasonally open marine facies in Barilari Bay are identified as diatomaceous glaciomarine sediment with higher organic carbon content, and variable ice rafted debris (IRD) concentrations, with more IRD found in the inner fjord than the outer fjord [*Christ et al*., 2014], consistent with deposition models elsewhere on the western AP where icebergs are concentrated in the inner bay by prevailing winds [*Domack and Ishman*, 1993]. These deposits are found in thin layers near the tops of KC-54, KC-42, and JKC-52, in disturbed sediment at the top of JPC-126, at the base of JPC-126, and in the outer fjord cores (with the exception of the ice shelf facies described below).

Concentrations of magnetic minerals in the inner fjord seasonally open marine facies are lower and less variable than the grounding-line facies, despite having significantly higher concentrations of IRD, due to dilution from biogenic sedimentation. However, magnetic mineralogy is much more variable than the grounding-line facies, including horizons with significant EM1 contribution, which is not found in significant proportions in grounding-line or diamict facies.

Concentrations of magnetic minerals in the outer bay seasonally open marine facies tracks variable dilution by biogenic sedimentation with possible postdepositional alteration due to diagenesis. Variability in magnetic grain-size shows a down-core coarsening trend beginning around 100 cm composite depth (cmcd). However, as magnetic concentration does not change significantly until below 250 cmcd, changes in magnetic grain-size are likely a convolved signal of provenance changes, sediment transport changes, and diagenetic alteration. This is consistent with a coincident change in magnetic mineral assemblage, as tracked through our end-member model.

4.3.3. Edge-Proximal Ice Shelf Facies

The outer bay ice shelf facies, identified by *Christ et al*. [2014] as a change in particle size and drop in total organic carbon, are present near the top of JKC-55 and JTC-127. The signature of the edge-proximal ice shelf facies observed in the outer bay is distinct and is composed of homogenous PSD grains with significant contributions from EM1 and EM3, consistent with sorted fines representative of deposits from an ice shelf edge [*Domack and Harris*, 1998].

5. Discussion

5.1. End-Members as Provenance Tracers

For our discussion, we interpret the end-member magnetic assemblages as tracers of changes in source contributions to the fjord. This demonstrates the usefulness and sensitivity of magnetic minerals to characterize lithogenic sediments, as χ(T) can be measured rapidly across all facies in the fjord and can quantify subtle differences in mineral assemblage. We found that other methods of characterizing lithogenic sediments (e.g., lithic sand grain assemblages, iron-oxide morphology, and iron oxide Fe/Ti ratios, determined through energy dispersive spectrometry) were useful to determine the major sediment contributions to the fjord; however, in this location, these analyses only revealed slight differences between cores and were limited to lithologies with abundant coarse particles [*Reilly*, 2013].

The Curie temperature for EM3 is observed less often than EM2 from our limited observation of Northwestern AP bedrock samples (Figure 4). However, it is the dominant contributor to the magnetic minerals in diamict from KC-54 (Figure 5c). We therefore consider relative proportions of EM3 as a tracer for material sourced to the inner bay, particularly Lawrie glacier, and perhaps Weir and Bilgeri glaciers. We will refer to this as the "inner-bay" signature.

EM2 has a Curie temperature that is much more abundant in bedrock samples from the Northwestern AP. It is present in grounding-line facies in the inner and middle bay. We consider this assemblage to be sourced to the inner bay, but not diagnostic of an inner bay source, and thus will refer to it as a "Northwestern AP" signature.

EM1 is primarily found in the outer bay cores and in a few horizons of the seasonally open facies in JPC-126. Based on these spatial observations, we consider this the "outer bay" signature. We suspect the dominant source is the more coastal and outer basin proximal Otlet glacier; however, without any observations of this signature in bedrock samples, we cannot rule out an externally derived source from elsewhere on the AP.

5.2. A Mid Holocene to Late Holocene Record of Glacial History

The outer bay cores, JKC-55, JTC-127, and JPC-127, contain a continuous time series extending to at least the middle Holocene. Sediments from the AP are difficult to date due to large reservoir ages and limited datable material [see *Christ et al.*, 2014 for discussion]. However, the reservoir age used in this suite of cores (1390 ± 40 years) is determined from the ^{14}C age of surface foraminifera in the inner bay, which is well supported by excellent agreement with ^{210}Pb-based and ^{137}Cs-based chronology and coincident timing of the Barilari Bay LIA expression with anomalously cold Holocene temperatures in the WAIS Divide Ice Core [*Orsi et al.*, 2012; *WAIS Divide Project Members*, 2013; *Christ et al.*, 2014]. The age model used here is limited by availability of sufficient foraminifera to ^{14}C date, but has good age control from the present to about 4000 cal. yr BP. Below 4,000 cal. yr BP, the age model is based solely on extrapolation of sedimentation rates (Figure 6j) [*Christ et al.*, 2014].

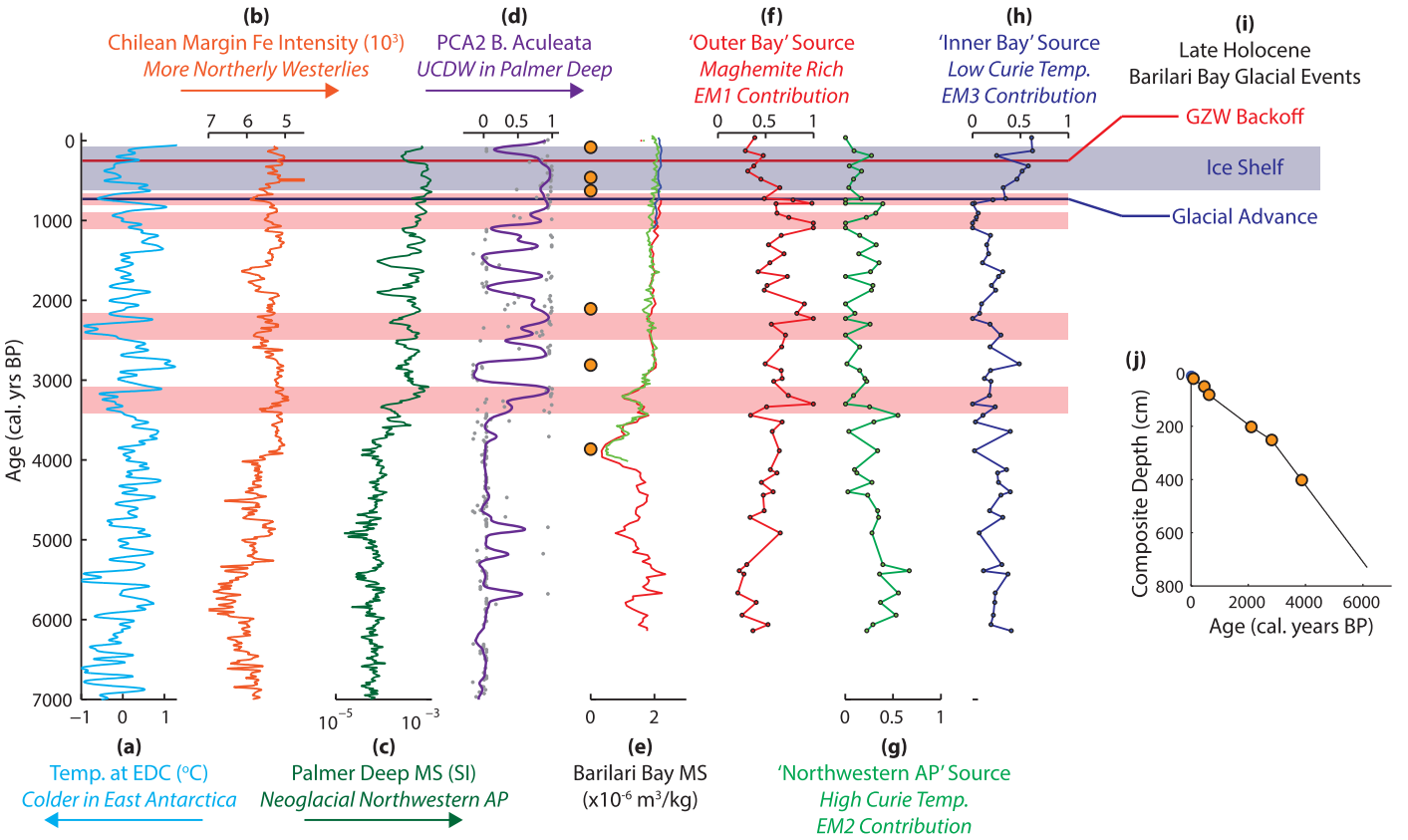

Figure 6. Mid Holocene to late Holocene climate proxies, including (a) surface air temperature of East Antarctica, reconstructed from the EPICA Dome C ice core and smoothed with a 50 year full width half max (FWHM) Gaussian filter [*Jouzel et al.*, 2007], (b) relative position of the westerly winds, inferred from iron content measured in counts per second (cps) on a sediment core from the southern Chilean margin smoothed with a 20 year FWHM Gaussian filter [*Lamy et al.*, 2001], (c) regional climate signal for the Northwestern AP presented as the magnetic susceptibility record from Palmer Deep [*Domack et al.*, 2001; *Brachfeld et al.*, 2002], (d) incursions of UCDW in Palmer Deep during the Neoglacial, tracked by the relative abundance of *B. aculeata* in Palmer Deep smoothed with a 100 year FWMH Gaussian filter [*Ishman and Sperling*, 2002], (e) χ_{lf} for JKC-55 (green), JTC-127 (blue), and JPC-127 (red) and locations of ^{14}C dates (orange dots), (f) relative proportion of EM1, the "outer bay" signature, (g) relative proportion of EM2, the "Northwestern AP" signature, (h) relative proportion of EM3, the "inner bay" signature. (i) Timing of the LIA inner bay glacial advance (horizontal blue line), establishment of an ice shelf (blue shading), and back-off from the grounding-line zone wedge (GZW; horizontal red line) in Barilari Bay [*Christ et al.*, 2014]. (j) Age model for the outer bay cores on their composite depth scale [*Christ et al.*, 2014]. Pink shading highlights the coldest mean intervals recognized in the EPICA Dome C ice core during the Northwestern AP Neoglacial.

The two most striking features of this provenance record in the outer bay cores are spikes in contribution from the "outer bay" source at roughly 750, 1000, 2200, and 3300 cal. yr BP and dominance of the "inner bay" source following the inner bay glacial advance documented in JPC-126 at about 730 cal. yr BP (Figures 6f–6h). We find the latter of these observations lends a great deal of support for an LIA ice shelf in Barilari Bay, as asserted by *Christ et al*. [2014] and interpret the fine magnetic grain-size, tracked by M_r/M_s (Figure 5a), and "inner bay" sourced sediment to be the sorted fines found at ice shelf edges in glaciomarine depositional models [*Domack and Harris*, 1998].

Signals of UCDW have been reported as consistently present on the western AP shelf during the early to mid-Holocene [*Shevenell and Kennett*, 2002; *Peck et al*., 2015], coincident with a more southerly position of the westerly winds reconstructed from the southern Chilean margin [*Lamy et al*., 2001] suggesting upwelling favorable conditions (Figure 6b). The mid-Holocene shift to a more northerly position in the westerly winds documented on the southern Chilean margin is roughly coincident with the large increase in magnetic susceptibility at Palmer Deep [*Domack et al*., 2001] and an increase in magnetic susceptibility at Barilari Bay (Figures 6c and 6e). Detailed rock magnetic work from Palmer Deep suggests this change in magnetic susceptibility is not primarily driven by diagenesis, as the change in susceptibility occurs roughly 10 m above the start of sulfate reduction [*Brachfeld and Banerjee*, 2000; *Brachfeld et al*., 2002]. Rather this change reflects changes in sediment provenance, glacial dynamics, and variable productivity cycles, coinciding with variability of UCDW incursion during the late Holocene, and is often interpreted as the transition from mid-Holocene warmth to Neoglacial conditions [*Brachfeld and Banerjee*, 2000; *Brachfeld et al*., 2002; *Shevenell and Kennett*, 2002].

Barilari Bay offers a glacial proximal fjord perspective on this transition from mid-Holocene warmth to Neoglacial conditions. The transition to Neoglacial conditions, as defined through magnetic susceptibility, is roughly coeval in Barilari Bay and reflects glacial advance of local glaciers and decreased primary productivity, as tracked by diatom abundance [*Christ et al*., 2014]. The spikes in "outer bay" sourced sediment between the onset of Neoglacial conditions and the start of LIA conditions occur coeval with high mean abundances of *Bulimina aculeata* dominated bethic foraminifera assemblages during the Neoglacial at ODP Site 1098 [*Ishman and Sperling*, 2002], suggesting frequent UCDW incursions to the Palmer Deep Basin and Barilari Bay through their shared pathway, the Hugo Island Trough [*Lavoie et al*., 2015]. We note that the Palmer Deep TEX_{86} sea surface reconstruction does not show warming during these events [*Shevenell et al*., 2011], consistent with the observed sensitivity of West Antarctic marine terminating glaciers to subsurface warming from UCDW upwelling, rather than surface warming [*Pritchard et al*., 2012; *Cook et al*., 2016].

Interestingly, the timing of these Neoglaical UCDW incursions and the increased "outer bay" sediments coincide with the coldest periods of late Holocene temperatures reconstructed in Eastern Antarctica in the EPICA Dome C ice core [*Jouzel et al*., 2007]. Based on data from instrumental records and high resolution reconstructions that are available for the last millennium, the SAM is characterized by a strong negative correlation in surface air temperatures between East Antarctica (especially at EPICA Dome C) and the Antarctic Peninsula [*Kwok and Comiso*, 2002; *Abram et al*., 2014]. We therefore argue the spikes in "outer bay" derived sediments are a response of smaller outer bay glaciers, especially Otlet glacier, in their advanced Neoglacial positions to periods of positive mean SAM-like states superimposed on the longer term Holocene trend of Westerly Wind position, which would impose upwelling favorable conditions and reduce sea ice, as observed through oceanographic measurements during the modern shift to a more positive SAM state [*Martinson et al*., 2008].

6. Conclusions

Magnetic mineralogy offers a powerful tracer for lithogenic sediments in Barilari Bay, reflecting the interplay of sediment province, transport processes, and primary productivity, and offering new insights to late Holocene atmosphere-ocean-glacial dynamics on the western AP. The magnetic mineral assemblages defined from fjord sediments can be interpreted within the context of limited bedrock observations and fjord sediment spatial distribution. Continued work around the AP and other regions to expand our knowledge of source region signatures will greatly improve our understanding of the origin and fate of terrigenous material on glaciated margins. We demonstrate strong evidence through magnetic tracers to support sedimentological identification of an LIA ice shelf in the fjord and provide new

insight to the sensitivity of glaciers in their advanced Neoglacial state to conditions akin to positive mean SAM state.

Acknowledgments

We thank the former Raytheon Polar services (now Lockheed Martin) shipboard team, the LARISSA science team, and the captain and crew of the *RV Nathaniel B. Palmer* for their efforts during NBP10-01. E. Domack, A. Leventer, S. Ishman, J. Wellner, B. Huber, K.C. Yoo, A. Christ, N. Elking, M. Talia Murray, S.M. Jeong, and A. Bianchi were instrumental in the recovery and characterization of the cores used in this study. This paper greatly benefited from discussions with R. Hatfield and C. Buizert. We thank A. Grunow, curator of the U.S. Polar Rock Repository (PRR), for her assistance and support in identifying and supplying bedrock samples. This research used samples and data provided by PRR at the Byrd Polar Research Institute, Ohio State University. The PRR is sponsored by the National Science Foundation Office of Polar Programs (NSF-OPP). This research also used samples provided by the Antarctic Marine Geology Research Facility (AMGRF) at Florida State University. The AMGRF is sponsored by the U.S. National Science Foundation. We thank Fabio Florindo and an anonymous reviewer for their helpful comments. This research was funded by NSF-OPP grant 0732605 and by NSF-MRI grants 0521069 and 0619402. B. Reilly is thankful to the ARCS Foundation Oregon Chapter for their generous support. Data are available in supporting information Tables S1–S13.

References

Abram, N. J., R. Mulvaney, F. Vimeux, S. J. Phipps, J. Turner, and M. H. England (2014), Evolution of the Southern Annular Mode during the past millennium, *Nat. Clim. Change*, *4*(7), 564–569, doi:10.1038/nclimate2235.

Adie, R. (1969a), Geologic map of Antarctica: Sheet 1, plate 1, folio 12, Northern Antarctic Peninsula, in *Antarctic Map Folio Series*, Am. Geogr. Soc., New York.

Adie, R. (1969b), Geologic map of Antarctica: Sheet 2, plate 2, folio 12, Southern Antarctic Peninsula, in *Antarctic Map Folio Series*, Am. Geogr. Soc., New York.

Bentley, M. J., et al. (2009), Mechanisms of Holocene palaeoenvironmental change in the Antarctic Peninsula region, *The Holocene*, *19*(1), 51–69, doi:10.1177/0959683608096603.

Bioucas-Dias, J. (2009), A variable splitting augmented Lagrangian approach to linear spectral unmixing, in *Hyperspectral Image and Signal Processing: Evolution in Remote Sensing*, pp. 1–4, WHISPERS'09, Inst. of Electr. and Electron. Eng., Piscataway, N. J., doi:10.1109/WHISPERS.2009.5289072.

Brachfeld, S. A. (2006), High-field magnetic susceptibility (χHF) as a proxy of biogenic sedimentation along the Antarctic Peninsula, *Phys. Earth Planet. Inter.*, *156*(3–4), 274–282, doi:10.1016/j.pepi.2005.06.019.

Brachfeld, S., and S. K. Banerjee (2000), Rock-magnetic carriers of century-scale susceptibility cycles in glacial-marine sediments from the Palmer Deep, Antarctic Peninsula, *Earth Planet. Sci. Lett.*, *176*(3–4), 443–455, doi:10.1016/S0012-821X(00)00008-X.

Brachfeld, S. A., S. K. Banerjee, Y. Guyodo, and G. D. Acton (2002), A 13200 year history of century to millennial-scale paleoenvironmental change magnetically recorded in the Palmer Deep, western Antarctic Peninsula, *Earth Planet. Sci. Lett.*, *194*(3), 311–326.

Brachfeld, S., A. M. Grunow, and E. Youcha (2004), Magnetic granulometry of igneous and metasedimentary rocks from northern Graham Land, Antarctic Peninsula, *Antarct. J. U. S.*, *33*, 298–303.

Brachfeld, S., J. Pinzon, J. Darley, L. Sagnotti, G. Kuhn, F. Florindo, G. Wilson, C. Ohneiser, D. Monien, and L. Joseph (2013), Iron oxide tracers of ice sheet extent and sediment provenance in the ANDRILL AND-1B drill core, Ross Sea, Antarctica, *Global Planet. Change*, *110*, 420–433, doi:10.1016/j.gloplacha.2013.09.015.

Burton-Johnson, A., and T. R. Riley (2015), Autochthonous v. accreted terrane development of continental margins: A revised in situ tectonic history of the Antarctic Peninsula, *J. Geol. Soc.*, *172*(6), 822–835, doi:10.1144/jgs2014-110.

Christ, A. J., et al. (2014), Late Holocene glacial advance and ice shelf growth in Barilari Bay, Graham Land, west Antarctic Peninsula, *Geol. Soc. Am. Bull.*, *127*(1–2), 297–315.

Cook, A. J., T. Murray, A. Luckman, D. G. Vaughan, and N. E. Barrand (2012), A new 100-m Digital Elevation Model of the Antarctic Peninsula derived from ASTER Global DEM: Methods and accuracy assessment, *Earth Syst. Sci. Data*, *4*(1), 129–142, doi:10.5194/essd-4-129-2012.

Cook, A. J., P. R. Holland, M. P. Meredith, T. Murray, A. Luckman, and D. G. Vaughan (2016), Ocean forcing of glacier retreat in the western Antarctic Peninsula, *Science*, *353*(6296), 283–286, doi:10.1126/science.aae0017.

Cowan, E. A., S. A. Brachfeld, R. D. Powell, and S. C. Schoolfield (2006), Terrane-specific rock magnetic characteristics preserved in glacimarine sediment from southern coastal Alaska, *Can. J. Earth Sci.*, *43*, 1269–1282.

Day, R., M. Fuller, and V. Schmidt (1977), Hysteresis properties of titanomagnetites, grain size and compositional dependence, *Phys. Earth Planet. Inter.*, *13*(4), 260–267.

Domack, E. W., and S. Ishman (1993), Oceanographic and physiographic controls on modern sedimentation within Antarctic fjords, *Geol. Soc. Am. Bull.*, *105*(9), 1175–1189, doi:10.1130/0016-7606(1993)105<1175:OAPCOM>2.3.CO;2.

Domack, E. W., and P. T. Harris (1998), A new depositional model for ice shelves, based upon sediment cores from the Ross Sea and the Mac. Robertson shelf, Antarctica, *Ann. Glaciol.*, *27*, 281–284.

Domack, E., A. Leventer, R. Dunbar, F. Taylor, S. Brachfeld, and C. Sjunneskog (2001), Chronology of the Palmer Deep site, Antarctic Peninsula: A Holocene palaeoenvironmental reference for the circum-Antarctic, *The Holocene*, *11*(1), 1–9, doi:10.1191/095968301673881493.

Domack, E., D. Duran, A. Leventer, S. Ishman, S. Doane, S. McCallum, D. Amblas, J. Ring, R. Gilbert, and M. Prentice (2005), Stability of the Larsen B ice shelf on the Antarctic Peninsula during the Holocene epoch, *Nature*, *436*(7051), 681–685, doi:10.1038/nature03908.

Elliot, D. H. (1975), Tectonics of Antarctica: A review, *Am. J. Sci.*, *275*(A), 45–106.

Ferraccioli, F., P. C. Jones, A. P. M. Vaughan, and P. T. Leat (2006), New aerogeophysical view of the Antarctic Peninsula: More pieces, less puzzle, *Geophys. Res. Lett.*, *33*, L05310, doi:10.1029/2005GL024636.

Gehring, A. U., H. Fischer, M. Louvel, K. Kunze, and P. G. Weidler (2009), High temperature stability of natural maghemite: A magnetic and spectroscopic study, *Geophys. J. Int.*, *179*, 1361–1371, doi:10.1111/j.1365-246X.2009.04348.x.

Golynsky, A., et al. (2013), Air and shipborne magnetic surveys of the Antarctic into the 21st century, *Tectonophysics*, *585*, 3–12, doi:10.1016/j.tecto.2012.02.017.

Hatfield, R. (2014), Particle size-specific magnetic measurements as a tool for enhancing our understanding of the bulk magnetic properties of sediments, *Minerals*, *4*(4), 758–787, doi:10.3390/min4040758.

Hatfield, R. G., J. S. Stoner, A. E. Carlson, A. V. Reyes, and B. A. Housen (2013), Source as a controlling factor on the quality and interpretation of sediment magnetic records from the northern North Atlantic, *Earth Planet. Sci. Lett.*, *368*, 69–77, doi:10.1016/j.epsl.2013.03.001.

Heslop, D. (2015), Numerical strategies for magnetic mineral unmixing, *Earth Sci. Rev.*, *150*, 256–284, doi:10.1016/j.earscirev.2015.07.007.

Heslop, D., and M. Dillon (2007), Unmixing magnetic remanence curves without *a priori* knowledge, *Geophys. J. Int.*, *170*(2), 556–566, doi:10.1111/j.1365-246X.2007.03432.x.

Heslop, D., and A. P. Roberts (2012), A method for unmixing magnetic hysteresis loops, *J. Geophys. Res.*, *117*, B03103, doi:10.1029/2011JB008859.

Hulbe, C. L., T. A. Scambos, T. Youngberg, and A. K. Lamb (2008), Patterns of glacier response to disintegration of the Larsen B ice shelf, Antarctic Peninsula, *Global Planet. Change*, *63*(1), 1–8, doi:10.1016/j.gloplacha.2008.04.001.

Ishman, S. E., and M. R. Sperling (2002), Benthic foraminiferal record of Holocene deep-water evolution in the Palmer Deep, western Antarctic Peninsula, *Geology*, *30*(5), 435–438.

Jouzel, J., et al. (2007), Orbital and millennial Antarctic climate variability over the past 800,000 years, *Science*, *317*(5839), 793–796, doi:10.1126/science.1141038.

Jovane, L., and K. L. Verosub (2011), Magnetic properties of Oligocene-Eocene cores from SHALDRIL II, Antarctica, in *Tectonic, Climatic, and Cryospheric Evolution of the Antarctic Peninsula*, edited by J. B. Anderson and J. S. Wellner, pp. 115–130, AGU, Washington, D. C.

Kwok, R., and J. C. Comiso (2002), Spatial patterns of variability in Antarctic surface temperature: Connections to the Southern Hemisphere Annular Mode and the Southern Oscillation, *Geophys. Res. Lett.*, *29*(14), doi:10.1029/2002GL015415.
Lamy, F., D. Hebbeln, U. Röhl, and G. Wefer (2001), Holocene rainfall variability in southern Chile: A marine record of latitudinal shifts of the Southern Westerlies, *Earth Planet. Sci. Lett.*, *185*(3–4), 369–382, doi:10.1016/S0012-821X(00)00381-2.
Lascu, I., R. J. Harrison, Y. Li, J. R. Muraszko, J. E. T. Channell, A. M. Piotrowski, and D. A. Hodell (2015), Magnetic unmixing of first-order reversal curve diagrams using principal component analysis, *Geochem. Geophys. Geosyst.*, *16*, 2900–2915, doi:10.1002/2015GC005909.
Lattard, D., R. Engelmann, A. Kontny, and U. Sauerzapf (2006), Curie temperatures of synthetic titanomagnetites in the Fe-Ti-O system: Effects of composition, crystal chemistry, and thermomagnetic methods, *J. Geophys. Res.*, *111*, B12S28, doi:10.1029/2006JB004591.
Lavoie, C., et al. (2015), Configuration of the Northern Antarctic Peninsula Ice Sheet at LGM based on a new synthesis of seabed imagery, *The Cryosphere*, *9*, 613–629, doi:10.5194/tc-9-613-2015.
Lees, J. A. (1997), Mineral magnetic properties of mixtures of environmental and synthetic materials: Linear additivity and interaction effects, *Geophys. J. Int.*, *131*(2), 335–346, doi:10.1111/j.1365-246X.1997.tb01226.x.
Leventer, A., E. W. Domack, S. E. Ishman, S. Brachfeld, C. E. McClennen, and P. Manley (1996), Productivity cycles of 200–300 years in the Antarctic Peninsula region: Understanding linkages among the sun, atmosphere, oceans, sea ice, and biota, *Geol. Soc. Am. Bull.*, *108*(12), 1626–1644.
Liu, Q., A. P. Roberts, J. C. Larrasoaña, S. K. Banerjee, Y. Guyodo, L. Tauxe, and F. Oldfield (2012), Environmental magnetism: Principles and applications, *Rev. Geophys.*, *50*, RG4002, doi:10.1029/2012RG000393.
Martinson, D. G., S. E. Stammerjohn, R. A. Iannuzzi, R. C. Smith, and M. Vernet (2008), Western Antarctic Peninsula physical oceanography and spatio-temporal variability, *Deep Sea Res., Part II*, *55*(18–19), 1964–1987, doi:10.1016/j.dsr2.2008.04.038.
Moyes, A. B. (1986), The Jinks Island complex: Magma mixing in a high-level intrusion from the Biscoe Islands, Antarctic Peninsula, *Br. Antarct. Surv. Bull.*, *70*, 55–69.
Orsi, A. J., B. D. Cornuelle, and J. P. Severinghaus (2012), Little Ice Age cold interval in West Antarctica: Evidence from borehole temperature at the West Antarctic Ice Sheet (WAIS) Divide, *Geophys. Res. Lett.*, *39*, L09710, doi:10.1029/2012GL051260.
Özdemir, Ö., and S. K. Banerjee (1984), High temperature stability of maghemite (γ-Fe_2O_3), *Geophys. Res. Lett.*, *11*(3), 161–164, doi:10.1029/GL011i003p00161.
Paillard, D., L. Labeyrie, and P. Yiou (1996), Macintosh program performs time-series analysis, *Eos Trans. AGU*, *77*(39), 379.
Peck, V. L., C. S. Allen, S. Kender, E. L. McClymont, and D. A. Hodgson (2015), Oceanographic variability on the West Antarctic Peninsula during the Holocene and the influence of upper circumpolar deep water, *Quat. Sci. Rev.*, *119*, 54–65, doi:10.1016/j.quascirev.2015.04.002.
Pritchard, H. D., S. R. M. Ligtenberg, H. A. Fricker, D. G. Vaughan, M. R. van den Broeke, and L. Padman (2012), Antarctic ice-sheet loss driven by basal melting of ice shelves, *Nature*, *484*(7395), 502–505, doi:10.1038/nature10968.
Razik, S., M. J. Dekkers, and T. von Dobeneck (2014), How environmental magnetism can enhance the interpretational value of grain-size analysis: A time-slice study on sediment export to the NW African margin in Heinrich Stadial 1 and Mid Holocene, *Palaeogeogr. Palaeoclimatol. Palaeoecol.*, *406*, 33–48, doi:10.1016/j.palaeo.2014.04.009.
Rebesco, M., et al. (2014), Boundary condition of grounding lines prior to collapse, Larsen-B Ice Shelf, Antarctica, *Science*, *345*(6202), 1354–1358, doi:10.1126/science.1256697.
Reilly, B. (2013), Climate evolution of the Antarctic Peninsula over the last 1,000 years: An environmental magnetism analysis of two high resolution sediment cores, MS thesis, Dep. of Earth and Environ. Stud., Montclair State Univ., Upper Monclair, N. J.
Roberts, A. P., L. Sagnotti, F. Florindo, S. M. Bohaty, K. L. Verosub, G. S. Wilson, and J. C. Zachos (2013), Environmental magnetic record of paleoclimate, unroofing of the Transantarctic Mountains, and volcanism in late Eocene to early Miocene glaci-marine sediments from the Victoria Land Basin, Ross Sea, Antarctica, *J. Geophys. Res. Solid Earth*, *118*, 1845–1861, doi:10.1002/jgrb.50151.
Sagnotti, L., F. Florindo, K. L. Verosub, G. S. Wilson, and A. P. Roberts (1998), Environmental magnetic record of Antarctic palaeoclimate from Eocene/Oligocene glaciomarine sediments, Victoria Land Basin, *Geophys. J. Int.*, *134*(3), 653–662, doi:10.1046/j.1365-246x.1998.00559.x.
Scambos, T., C. Hulbe, and M. Fahnestock (2003), Climate-induced ice shelf disintegration in the Antarctic peninsula, in *Antarctic Peninsula Climate Variability: Historical and Paleoenvironmental Perspectives*, edited by E. Domack, pp. 79–92, AGU, Washington, D. C.
Shevenell, A. E., and J. P. Kennett (2002), Antarctic Holocene climate change: A benthic foraminiferal stable isotope record from Palmer Deep, *Paleoceanography*, *17*(2), doi:10.1029/2000PA000596.
Shevenell, A. E., A. E. Ingalls, E. W. Domack, and C. Kelly (2011), Holocene Southern Ocean surface temperature variability west of the Antarctic Peninsula, *Nature*, *470*(7333), 250–254, doi:10.1038/nature09751.
Smellie, J. L., A. B. Moyes, P. D. Marsh, and J. W. Thomson (1985), Reports on Antarctic field Work. Geology of Hugo Island, Quintana Island, Sooty Rock, Betbeder Islands and parts of the Biscoe and Outcast Islands, *Br. Antarct. Surv. Bull.*, (68), 91–100.
Smith, R. C., et al. (1999), Marine ecosystem sensitivity to climate change historical observations and paleoecological records reveal ecological transitions in the Antarctic Peninsula region, *BioScience*, *49*(5), 393–404, doi:10.2307/1313632.
Stober, J. C., and R. Thompson (1979), An investigation into the source of magnetic minerals in some Finnish lake sediments, *Earth Planet. Sci. Lett.*, *45*(2), 464–474, doi:10.1016/0012-821X(79)90145-6.
Stoner, J. S., J. E. Channell, and C. Hillaire-Marcel (1995), Magnetic properties of deep-sea sediments off southwest Greenland: Evidence for major differences between the last two deglaciations, *Geology*, *23*(3), 241–244.
Stoner, J. S., J. E. Channell, and C. Hillaire-Marcel (1996), The magnetic signature of rapidly deposited detrital layers from the deep Labrador Sea: Relationship to North Atlantic Heinrich layers, *Paleoceanography*, *11*(3), 309–325.
Vaughan, D. G. (2006), Recent trends in melting conditions on the Antarctic Peninsula and their implications for ice-sheet mass balance and sea level, *Arct. Antarct. Alp. Res.*, *38*(1), 147–152.
Venuti, A. F., F. Florindo, A. Caburlotto, M. W. Hounslow, C. D. Hillenbrand, E. Strada, F. M. Talarico, and A. Cavallo (2011), Late Quaternary sediments from deep-sea sediment drifts on the Antarctic Peninsula Pacific margin: Climatic control on provenance of minerals, *J. Geophys. Res.*, *116*, B06104, doi:10.1029/2010JB007952.
Verosub, K. L., and A. P. Roberts (1995), Environmental magnetism: Past, present, and future, *J. Geophys. Res.*, *100*(B2), 2175–2192.
WAIS Divide Project Members (2013), Onset of deglacial warming in West Antarctica driven by local orbital forcing, *Nature*, *500*(7463), 440–444, doi:10.1038/nature12376.
Wendt, A. S., A. P. M. Vaughan, F. Ferraccioli, and A. M. Grunow (2013), Magnetic susceptibilities of rocks of the Antarctic Peninsula: Implications for the redox state of the batholith and the extent of metamorphic zones, *Tectonophysics*, *585*, 48–67, doi:10.1016/j.tecto.2012.07.011.